Rotationally resolved photoionization: Influence of the 4σ→kσ shape resonance on CO + (B 2 Σ +) rotational distributions

George R. Farquar, J. Scott Miller, E. D. Poliakoff, Kwanghsi Wang, and V. McKoy

Citation: The Journal of Chemical Physics **115**, 9764 (2001); doi: 10.1063/1.1415463
View online: http://dx.doi.org/10.1063/1.1415463
View Table of Contents: http://scitation.aip.org/content/aip/journal/jcp/115/21?ver=pdfcov
Published by the AIP Publishing

Rotationally resolved photoionization: Influence of the $4\sigma \rightarrow k\sigma$ shape resonance on $CO^+(B\ ^2\Sigma^+)$ rotational distributions

George R. Farquar, J. Scott Miller, and E. D. Poliakoff[a)]
Department of Chemistry, Louisiana State University, Baton Rouge, Louisiana 70803

Kwanghsi Wang and V. McKoy
Arthur Amos Noyes Laboratory of Chemical Physics, California Institute of Technology, Pasadena, California 91125

(Received 10 May 2001; accepted 12 September 2001)

We present experimental and theoretical results on rotational distributions of $CO^+(B\ ^2\Sigma^+)$ photoions. Rotational distributions were determined for both the $v^+=0$ and $v^+=1$ vibrational levels following photoionization of cold ($T_0 \approx 9$ K) neutral CO target molecules. Data were generated using dispersed ionic fluorescence over a wide range of photoelectron kinetic energies, $0 \leqslant E_k \leqslant 120$ eV, which allows one to interrogate the ionization dynamics. This wide spectral coverage permits illustrative comparisons with theory, and calculated spectra are presented to interpret the data. In particular, the comparison between theory and experiment serves to identify the strong continuum resonant enhancement at $h\nu_{\mathrm{exc}} \approx 35$ eV in the $l=3$ partial wave of the $4\sigma \rightarrow k\sigma$ ionization channel, as this feature has profound effects on the ion rotational distributions over a wide range of energy. Second, there are differences between the rotational substructure for the $v^+=0$ and $v^+=1$ vibrational levels. All of the experimentally observed features and trends are reproduced by theory, and the consequences of these comparisons are discussed. © *2001 American Institute of Physics.* [DOI: 10.1063/1.1415463]

I. INTRODUCTION

Molecular photoionization is frequently dominated by a single partial wave in localized regions of the ionization continuum. Because of the coupling between the angular momentum of the photoelectron and that of molecular rotation during photoionization, measurements of rotational distributions provide insights into the dynamics of the photoelectron escape, i.e., the angular momentum composition of the continuum wave function as well as the exchange of angular momentum between the photoelectron and the ion core.[1–3] However, processes in the ionization continuum frequently span a wide spectral range. For example, Cooper minima[4–8] and shape resonances[9–16] typically extend over a range of 10–50 eV, and it is hence desirable to study rotational distributions over a comparable range. Unfortunately, rotationally resolved photoelectron experiments are typically limited to the near-threshold region[17–27] (although recent progress has resulted in partially rotationally resolved photoelectron data over a significant range[28,29]). In our previous studies, we demonstrated that dispersed fluorescence is capable of determining energy-dependent aspects of rotationally resolved effects in molecular photoionization over the broadest energy range.[30–35] In particular, we showed that rotational distributions in N_2 photoionization were strongly influenced by Cooper minima in the $l=2$ partial wave of the $2\sigma_u \rightarrow k\sigma_g$ channel over a 250 eV range.[32–35] An interesting and unexpected result of those previous studies was that the rotationally resolved characteristics of $N_2\ 2\sigma_u^{-1}$ and $CO\ 4\sigma^{-1}$ photoionization were qualitatively different for these valence isoelectronic systems. The differences were attributed to qualitative differences in their ionization continua. In the case of N_2, there are Cooper minima in the $2\sigma_u \rightarrow k\sigma_g$ channel at high energies ($h\nu_{\mathrm{exc}} > 100$ eV) but no shape resonances, while for CO, there is a strong $4\sigma \rightarrow k\sigma$ shape resonance near threshold. While the qualitative energy dependences of the two systems were distinctly different, there were no clear signatures of the shape resonance for the CO case, i.e., the rotational distributions were comparatively flat in both the measured and calculated spectra. This lack of a conspicuous marker for rotational consequences of a high angular momentum shape resonance was attributed to the relatively hot target molecules ($T_0 \approx 18$ K), which washed out the effects of the shape resonance. In this paper, we show that the effects of the $CO\ 4\sigma \rightarrow k\sigma$ shape resonance can be amplified and studied quantitatively if the target molecules are cooled more effectively. The excitation and fluorescence sequence employed for the current study is summarized by Eq. (1).

$$\begin{aligned} &CO(X\ ^1\Sigma^+, v_0=0, \{N_0\}) + h\nu_{\mathrm{exc}} \\ &\quad \rightarrow CO^+(B\ ^2\Sigma^+, v^+, N^+) + e^- \\ &\qquad \downarrow \\ &\qquad CO^+(X\ ^2\Sigma^+, v'', N'') + h\nu_{v^+ v'' N^+ N''}. \end{aligned} \tag{1}$$

A "0" subscript denotes a target level undergoing ionization, and a double-prime superscript is used to describe the lower level in the fluorescence transition. The notation $\{N_0\}$ indicates that there is a thermal distribution of populated target rotational levels. A key aspect of dispersed fluorescence measurements is that the detection bandwidth is decoupled from

a)Author to whom correspondence should be addressed. Electronic mail: epoliak@lsu.edu

the excitation bandwidth.[34,36] As a result, it is possible to acquire rotational distributions over a very wide spectral range. The disadvantage of the dispersed fluorescence method is that one cannot tell how an ionic level was created, so it is important to restrict the number of target levels undergoing ionization to allow for meaningful comparisons with theory. In this regard, the current investigation works with a colder distribution of target molecules than in the previous work.[32,33] Also, the current experiments determine the rotational substructure for both the $v^+=0$ and $v^+=1$ levels, in analogy with previous work on N_2.[37]

There have been numerous significant advances in rotationally resolved photoionization experiments in recent years, and the current study provides useful information for interpreting the data from other rotationally resolved experiments and placing the results into a broader context. For example, zero-kinetic-energy/pulsed field-ionization (ZEKE-PFI) spectroscopy has been the most common method to determine rotational distributions at the ionization threshold.[17–22,38–52] A related method is to employ REMPI coupled with photoelectron spectroscopy.[26,27,53–57] The resolution is not quite as high for such experiments, but the capability of determining angularly resolved photoelectron maps is extremely powerful. Indeed, this photoelectron mapping has developed into a useful tool for determining the angular momentum composition of the photoelectron wave function, as well as for studying the intramolecular ''alignment evolution'' dynamics.[58–61] However, all of these methods are restricted to the threshold, or the near-threshold region, and the current study shows that the spectral extent of the rotational changes can be substantial. In order to understand the photoelectron ''half-scattering'' dynamics, it is useful to understand how the photoion rotation varies with photoelectron energy, and dispersed fluorescence experiments on molecular photoions provide precisely this type of information.

II. EXPERIMENT

The experimental method has been described elsewhere[34,36,62] and only details pertinent to the present study are discussed here. A schematic of the apparatus is shown in Fig. 1. Synchrotron radiation is produced at the Center for Advanced Microstructures and Devices (CAMD),[63] Louisiana State University. Typical stored ring currents are 200 mA and the beam energy is 1.3 GeV. The resulting radiation is monochromatized ($\Delta h\nu \approx 0.4$ eV) by a 6-m plane grating monochromator[64] and ionizes the target molecules. Data collection times were typically 30 min per incident energy. The incident photons are channeled into the experimental chamber using a capillary light guide which is differentially pumped in two stages. The use of differential pumping is critical to maintain an ultrahigh vacuum in the beamline and storage ring (10^{-9} Torr), while maintaining the chamber at ca. 10^{-4} Torr. In order to limit the number of target states a supersonic expansion nozzle was used (100 μm) with a stagnation pressure of 4 psig. To enhance the rotational cooling, liquid nitrogen was used to refrigerate a copper jacket surrounding the gas jet. This enhancement significantly reduced the number of populated rotational target states. Obtaining rotational resolution is demanding for the $CO^+(B\,^2\Sigma^+ \rightarrow X\,^2\Sigma^+)$ transition, as rotational transitions are closely spaced.[33] To achieve the required resolving power, a 1-m optical monochromator was used (Instruments SA model THR-1000) with a 3600 g/mm grating. The slit width was set at 50 μm, resulting in a fluorescence bandwidth of 0.13 Å. For fluorescence detection a CCD-based OMA detector was used (Princeton Instruments LN/CCD-134/400-ES1). This detector employs a back-thinned chip which has a quantum efficiency roughly a factor of 2 better than that of the front-illuminated CCD employed in the previous work.[33] This provided qualitatively superior results and much faster data acquisition times (better than a factor of 2, owing to the background and read-noise effects inherent in any CD detector). Data were taken over the range from 20–140 eV. Data sets were collected with better counting statistics over a limited spectral range (20–40 eV) to allow for a detailed comparison for the rotational substructure between the $v^+=0$ and $v^+=1$ vibrational levels.

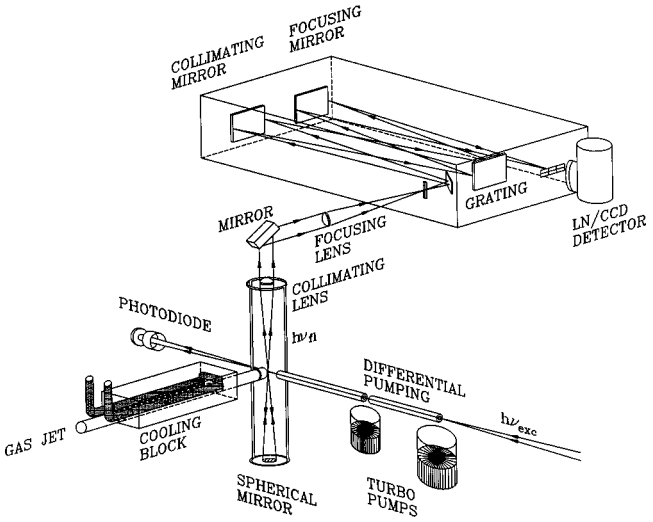

FIG. 1. Experimental schematic.

III. THEORY

The formulation of rotationally resolved photoelectron spectroscopy (used for comparisons with dispersed fluorescence experiments) has been described previously.[1,33,65] We briefly review the necessary background. These calculations were performed over a wider spectral range than is typical to obtain the ion distributions needed for comparison with the present experiments. Since the fluorescence experiment integrates over all initial rotational levels J_0, we consider all the transitions terminating in a specific ion level J^+. In the present case, ionization originating from each of the $(2J_0+1)$ magnetic sublevels of the ground state of CO forms an independent channel. The total cross section σ for ionization of a J_0 level of the state leading to a J^+ level of the ion can be written as

$$\sigma \propto \sum_{\substack{lm \\ M_{J_0},M_{J^+}}} \rho_{M_{J_0}M_{J_0}} |C_{lm}(M_{J_0},M_{J^+})|^2, \tag{2}$$

where $\rho_{M_{J_0}M_{J_0}}$ is the population of a specific M_{J_0} level of the ground state. The relative populations of the target rotational levels are governed by the supersonic expansion conditions. In our calculations, the initial J_0 rotational levels are assumed to be unaligned, i.e., all M_{J_0} sublevels of the J_0 level are equally populated. The coefficients $C_{lm}(M_{J_0},M_{J^+})$ of Eq. (2) are related to the probability for photoionization of the M_{J_0} level of the intermediate state leading to the M_{J^+} level of the ionic state. For Hund's case (b) coupling scheme, the $C_{lm}(M_{J_0},M_{J^+})$ coefficients have the form

$$C_{lm}(M_{J_0},M_{J^+})=\sqrt{\frac{4\pi}{3}}[(2N^+ +1)(2N_0+1)(2J_0+1)(2S_0+1)]^{1/2}\sum\,(-1)^P(2N_t+1)\begin{pmatrix} N_0 & S_0 & J_0 \\ M_0 & M_{S_0} & M_{J_0}\end{pmatrix}$$
$$\times\begin{pmatrix} N^+ & S^+ & J^+ \\ M^+ & M_{S^+} & -M_{J^+}\end{pmatrix}\begin{pmatrix} S^+ & 1/2 & S_0 \\ M_{S^+} & M_\sigma & -M_{S_0}\end{pmatrix}\begin{pmatrix} N^+ & N_0 & N_t \\ -M^+ & M_0 & m_t\end{pmatrix}\begin{pmatrix} N_t & 1 & l \\ -m_t & \mu_0 & -m\end{pmatrix}$$
$$\times\sum_{\substack{\mu \\ \lambda_t}}(-1)^{\Lambda^+-\mu}\hat{I}_{l\lambda\mu}\begin{pmatrix} N^+ & N_0 & N_t \\ -\Lambda^+ & \Lambda & \lambda_t\end{pmatrix}\begin{pmatrix} N_t & 1 & l \\ -\lambda_t & \mu & -\lambda\end{pmatrix}, \tag{3}$$

with

$$P=M^+ +M_{J^+}-M_0+\mu_0-N_0-N^+ +S_0+\tfrac{1}{2}, \tag{4}$$

where λ and m are projections of the photoelectron's angular momentum l in the molecular and laboratory frames, respectively, Λ is the projection of electronic orbital angular momentum along the internuclear axis, S is the total spin, R denotes a dependence on internuclear distance, $\tilde{I}_{l\lambda\mu}$ is the vibrationally averaged photoelectron matrix element between the ground state and the photoelectron continuum wave function, and μ and μ_0 are the light polarization indices in the molecular and laboratory frames, respectively. The symbols with superscript $+$ and subscript 0 are related to the same quantities in the ion and neutral molecule, respectively. The rotational temperature for the CO expansion is assumed to be 9 K. This temperature is determined by fitting to the experimental data, as described previously.[33] In our earlier work, we showed that the data analysis was not strongly dependent on the initial temperature of the neutral target molecules, and that is the case for the present study as well.

The degree of rotational excitation in the photoionization process is strongly influenced by the angular momentum composition of the photoelectron. As a result, a key quantity is the matrix element, $\mathrm{r}_{\mathrm{fi}}^{l\lambda\mu}(R)$, for photoionization from a bound orbital ϕ_i into a continuum orbital $\phi_{f,\mathbf{k}}^{(-)}(\mathbf{r},R)$ where $\mathbf{k}$ is the momentum of the photoelectron and $(-)$ denotes incoming-wave boundary conditions appropriate to photoionization. These R-dependent matrix elements are further vibrationally averaged to obtain the $\tilde{I}_{l\lambda\mu}$. Note that these matrix elements depend on the internuclear separation, and the calculations (described below) include this variation explicitly. This is significant for the current study, because the R dependence provides information on how the rotational substructure will differ between the $v^+=0$ and $v^+=1$ levels. In the calculation of the photoelectron matrix element, $\mathrm{r}_{\mathrm{fi}}^{l\lambda\mu}(R)$, one considers both l-conserving and l-changing collisions. Whereas only $l=l'$ would be allowed for the central fields of atomic systems, where the angular momentum of the photoelectron must be conserved, $l\neq l'$ terms arise in molecules due to angular momentum coupling brought about by the nonspherical molecular ion potential. These l-changing collisions strongly influence the ion rotational distributions in molecular photoionization. The present fluorescence measurements allow us to see how this underlying dynamical behavior evolves with energy.

There are two dipole-allowed channels for photoionization of the 4σ orbital of the ground-state CO. An electron from the 4σ orbital can be ejected into $k\sigma$ or $k\pi$ continuum channels. Ionization into the $k\sigma$ and $k\pi$ continua results in an electron–ion complex of $^1\Sigma^+$ and $^1\Pi$ total final-state symmetries, respectively. The procedures for determining the continuum wave functions are described in detail elsewhere.[2] Our calculations are performed at the Hartree–Fock level, which is sufficient to identify and account for the key dynamical aspects here. The ground-state wave function of CO is obtained at the self-consistent-field (SCF) level and the Gaussian basis functions employed are the same as in Ref. 66. The angular momentum composition of the 4σ orbital of CO is 14.56%s, 62.35%p, 15.67%d, 3.09%f, 2.72%g ($l_0=4$), 0.36%h ($l_0=5$), and 0.57%i ($l_0=6$) at $R_e=2.1322$ a.u. This 4σ orbital evolves with internuclear distance, as seen by examining the angular momentum composition at a couple of representative internuclear separations, e.g., the inner and outer turning points of the $v^+=1$ ionic level. At the inner turning point ($R=1.992$ a.u.), it has a dominant s, p, and d composition [17.06%s, 58.36%p, 18.24%d, 2.59%f, 2.51%g ($l_0=4$), 0.30%h ($l_0=5$), and 0.45%i ($l_0=6$)]. The p character grows with increasing internuclear separation. At the outer turning point ($R=2.305$ a.u.), the composition is 12.49%s, 66.93%p, 11.82%d, 3.73%f, 2.89%g ($l_0=4$), 0.45%h ($l_0=5$), and 0.71%i ($l_0=6$). For the final state, we assume a frozen-core Hartree–Fock model in which the ion orbitals are taken to be that of the ground state of CO and the photoelectron orbital is obtained as a solution of a one-electron Schrödinger equation. All matrix elements arising in the solution of the

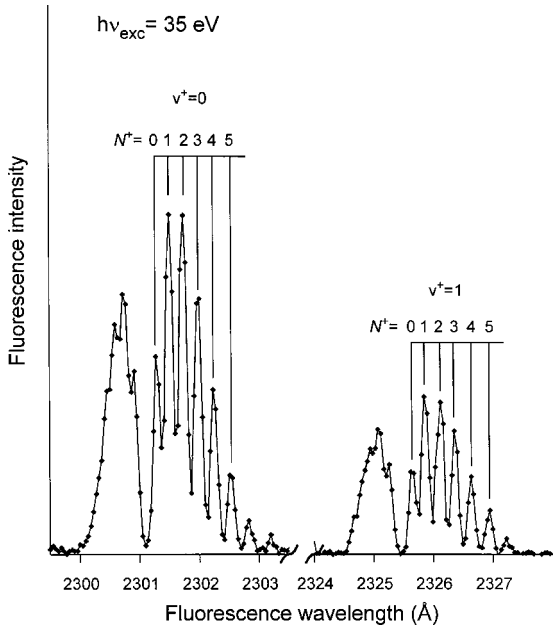

FIG. 2. Rotationally resolved fluorescence spectrum $CO^+(B\,^2\Sigma^+ \rightarrow X\,^2\Sigma^+)$ following CO $4\sigma^{-1}$ photoionization, with the upper rotational quantum number for each transition labeled.

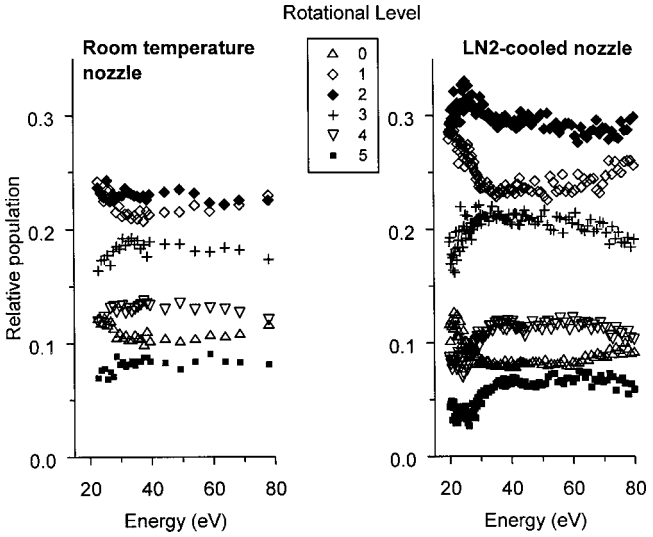

FIG. 3. Left-hand side: Rotational populations from previous study (Ref. 33). Right-hand side: Rotational populations from current study using cryogenically cooled supersonic nozzle. This figure illustrates that the improved cooling amplifies the magnitude of the variations in rotational populations, enabling systematic studies of the energy-dependent rotational effects of the continuum scattering dynamics.

Lippmann–Schwinger equation were evaluated via single-center expansions at the center of mass.

IV. RESULTS AND DISCUSSION

A typical $CO^+(B\,^2\Sigma^+ \rightarrow X\,^2\Sigma^+)$ fluorescence spectrum is shown in Fig. 2. The quality of the data is higher than for those reported previously,[32,33] in terms of both resolution and counting statistics. This is largely a result of the increased quantum efficiency of the CCD detector employed in the current study. The horizontal axis is split to display results for both $v^+=0$ and $v^+=1$. Both bands are obtained in a single exposure at each incident energy, so variations in experimental conditions have minimal effects when comparing results for these two vibrational levels. The intensities of the P-branch transitions were determined more precisely because of the greater separation between the peaks, so these intensities were used in the data analysis. To determine the relative populations, the intensity of each rotational transition was integrated, corrected for the rotational line strength, and the normalized totals were reported.[32,33] A plot of the relative populations as a function of photon energy is given in Fig. 3. In addition to the current results, data from the previous study[33] are shown on the left-hand side for comparison. The differences between the data sets demonstrate that the sample is rotationally colder in the present study. To see this, note that the relative populations of the lower rotational levels are enhanced while the higher rotational levels are reduced in the current study, which shows that the *ionic* rotational distribution is colder. The ionic rotational distribution is a reflection of the target distribution with photoionization rotational transitions folded in;[33] hence, Fig. 3 demonstrates that the neutral target distribution is colder as well. More importantly, Fig. 3 shows that the energy dependence for each rotational level population has more pronounced excursions in the present investigation. This indicates that fewer target rotational levels are populated and averaged over in the rotational distributions that are observed.[33] The most pronounced features in these curves are observed for photon energies below 50 eV. These excursions in the rotational distributions are the result of the shape resonance in the $4\sigma \rightarrow k\sigma$ $l=3$ channel.[67,68]

In Fig. 4, the energy dependence of each rotational level population is plotted in a separate frame and the trends are evident. Also shown in Fig. 4 are the results from theory for the $v^+=0$ rotational populations, which permit a comparison with experiment. There is excellent agreement between calculated and experimentally determined rotational populations. As discussed above, the relative rotational populations depend on the initial temperature of the target molecule undergoing photoionization.[33] Calculations were performed for several target rotational temperatures, and the agreement between experiment and theory was best when a target temperature of 9 K was used in the calculations. (Note that the baselines are offset, which amplifies the effects.) The lower rotational levels ($N^+=0$ and $N^+=1$) exhibit a sharp decrease near threshold, followed by a broad minimum between 30–60 eV photon energy. The $N^+=2$ and $N^+=3$ levels are comparatively flat, except for a sharp maximum near threshold (i.e., at $h\nu_{\mathrm{exc}} \approx 30$ eV). This is particularly apparent in the $N^+=2$ curve. Finally, the higher rotational levels ($N^+=4$ and $N^+=5$) exhibit a minimum near threshold ($h\nu_{\mathrm{exc}} \approx 25$ eV), followed by a maximum at 45 eV and a broad minimum at $h\nu_{\mathrm{exc}} \approx 100$ eV. These transitions followed not only the conservation of the angular momenta, but also the rotational selection rule of $\Delta N + l = odd$ which can be obtained from Eq. (3). Since many initial rotational levels are populated, all the partial wave components of the photoelectron contribute to each ion rotational level. Agreement between the measured and calculated spectra is quite good.

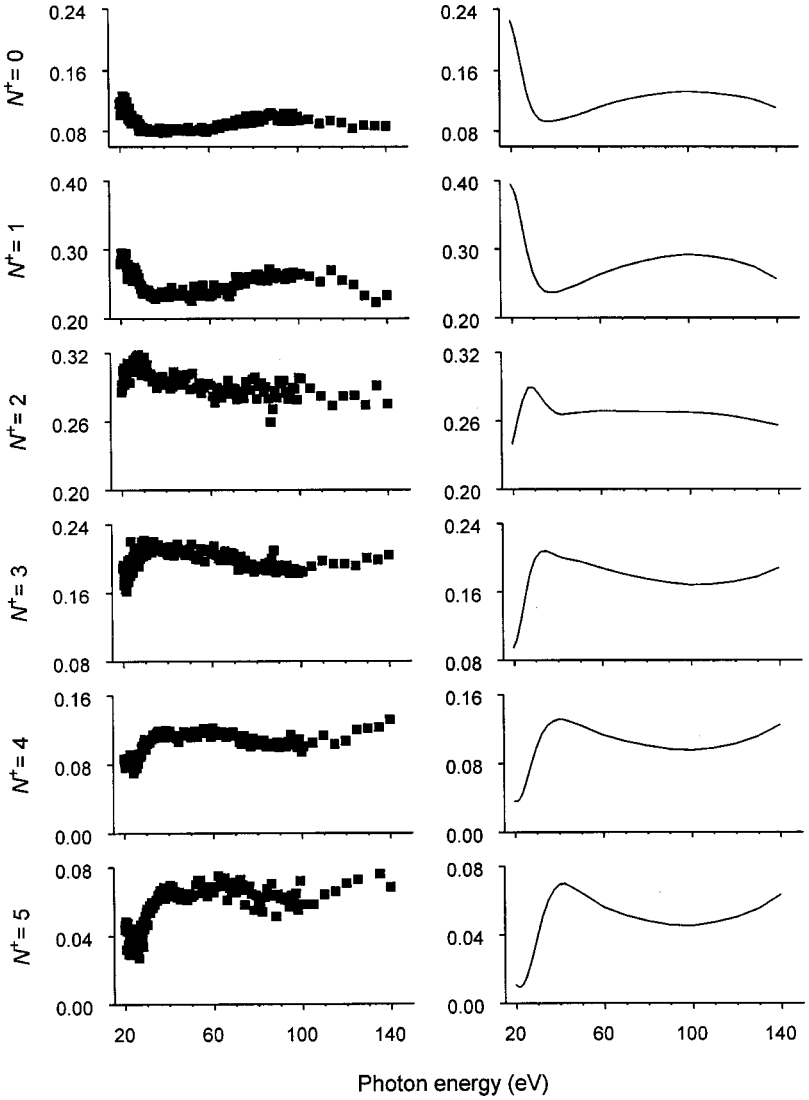

FIG. 4. Rotational populations as a function of energy (experimental and theoretical). Note the offset baselines. The trends are discussed in the text.

The primary motivation of this study was to see how the relative populations are modulated in the low-energy region. The results clearly demonstrate that the shape resonance in the $k\sigma$ channel affects the population of the ion rotational levels between 20–50 eV. To more closely examine this behavior, we show the calculated dipole amplitudes for the $4\sigma \rightarrow k\sigma$ channel in Fig. 5. It is clear that the strong resonance in the $l=3$ component coincides with the more pronounced excursions in the rotational populations in Fig. 4. With dominant p character ($\approx$62%) in the 4σ orbital of the ground state, strong s and d partial waves are expected to contribute to the photoionization on the basis of an atomic-like picture. Indeed, this is the case with stronger d wave contribution near threshold and stronger s wave at larger energies. In addition to the shape resonance ($l=3$), the p wave is also strong and comparable to that of the d wave. These strong p- and f waves may arise from the contributions of the s ($\approx$15%) and d ($\approx$16%) of the 4σ orbital or from the angular momentum coupling of the partial waves caused by the nonspherical ion potential. The photoionization process is quite molecular.

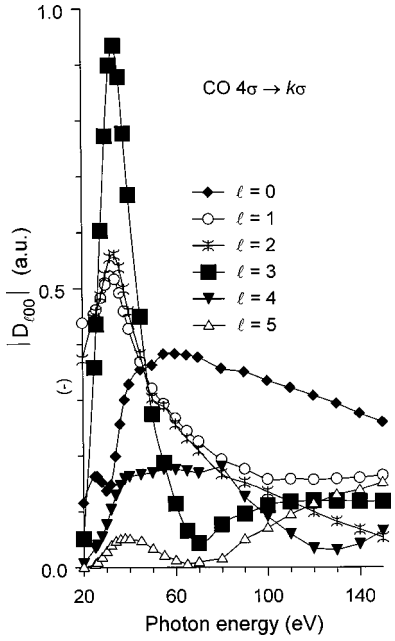

FIG. 5. Calculated partial wave amplitudes for the $4\sigma \rightarrow k\sigma$ continuum channel. Note the strong enhancement in the $l=3$ component.

It is also instructive to examine the higher energy behavior. In the earlier study, the relative populations were com-

paratively flat over a broad range. The present results demonstrate that the rotational populations for the lower (upper) rotational levels are clearly decreasing (increasing) at the highest photon energies. This behavior can be rationalized by noting that the contributions of larger angular momentum components increase with photoelectron energy. Large amplitudes for high-l partial waves make larger ΔN transitions possible. Thus, it is probably true that as the photon energy is increased over a broad enough range, all molecules will exhibit the same qualitative behavior—lower rotational levels decreasing and upper rotational levels increasing with increasing energy—as is observed in Fig. 4. Note the systematic excursions in the rotational populations in the higher energy region, e.g., the broad maximum at $h\nu \approx 100\,\mathrm{eV}$ in the $N^+=0$ curve. These features are due to the finer details of the growth of the higher-l components ($l=4$ and 5). These amplitudes behave as they do because of the existence of Cooper minima (50 eV for $l=5$, 135 eV for $l=4$), as can be seen in Fig. 5. As a result, the higher-l components are effectively suppressed at lower energies. The previous $N_2\, 2\sigma_u^{-1}$ results exhibited similar behavior in that the higher rotational levels grew in intensity with increasing photon energy.[32,33] However, while the global trends are similar to those of the N_2 results, it is important to note that the approach to this limiting behavior is much different for these valence isoelectronic systems. Thus, the limiting behavior might be similar, but if the approach to that limit is sufficiently gradual, then even the broad-range behavior (i.e., dynamics over a range of hundreds of eV) for these two systems can appear distinctly different.

The fluorescence spectrum (Fig. 2) displays transitions originating from the $v^+=1$ level as well as from the $v^+=0$ level. Thus, it possible to compare the rotational substructure between the two bands as a function of incident photon energy, analogous to a previous study on vibrational–rotational–electronic (V–R–E) correlations in $2\sigma_u^{-1}$ photoionization of N_2.[37] It is well known that the effects of shape resonances are influenced by the bond length for diatomic systems,[69,70] so it is reasonable to inquire if the rotational substructure would be affected, particularly in the lower energy region where the shape resonant effects are dominant. This comparison has been generated, and the results are shown in Fig. 6. The effects are relatively small, so the data are presented in a way to highlight the differences. Specifically, each frame in Fig. 6 corresponds to a specific rotational level of the ion, and the vertical axis represents the ratio of the relative population for that rotational level for the $v^+=1$ level relative to that of the $v^+=0$ level. The qualitative trends are reproduced well by theory, although the experimental results display significantly more scatter. Specifically, for a photon energy of $h\nu_{\mathrm{exc}} \approx 27\,\mathrm{eV}$, these ratios display peaks for the lower rotational levels and dips for the upper rotational levels. This is because the shape resonance shifts to lower energy as the bond length is increased. On average, the $v^+=1$ level samples greater internuclear separations than the $v^+=0$ level, and as a result, extrema in the rotationally resolved vibrational branching ratios are shifted to lower energy from the shape resonance position seen for the $l=3$ resonance displayed in Fig. 5. In general, the agreement between experiment and theory is very good for all of the results shown in Figs. 4 and 6, lending credibility to both the underlying theory and the experiment.

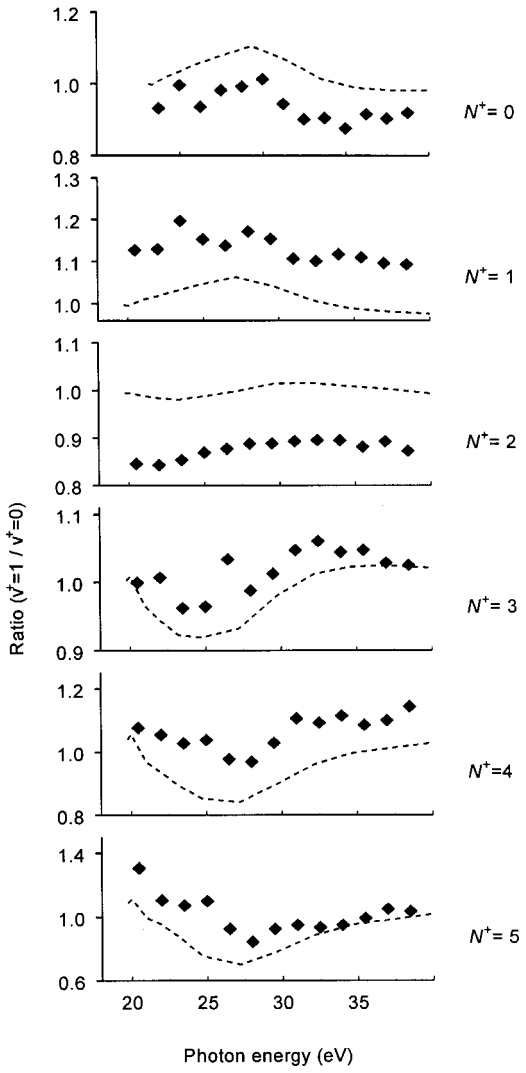

FIG. 6. Ratio of rotational populations for the $v^+=1$ to $v^+=0$ level.

V. CONCLUSIONS

Rotationally resolved results are presented for $4\sigma^{-1}$ photoionization of CO. Specifically, experiment and theory have been used to determine the relative rates of production of specific rotational levels of the $CO^+(B\,^2\Sigma^+)$ state. Experiments were performed by measuring the dispersed fluorescence from electronically excited photoions, and calculations were performed using Schwinger variational methods. The dependence of the rotational distributions as a function of incident photon energy has been determined over a very wide range, and the effects of a $4\sigma \rightarrow k\sigma$ shape resonance are clearly discernible in the data and in the theory. In fact, the agreement between experiment and theory is excellent. By comparing the present experimental results to previous data, it is demonstrated that improved rotational cooling of the neutral target molecules has significantly amplified the ef-

fects which are now visible. In so doing, the present study clarifies the global picture of rotational effects in molecular photoionization scattering dynamics.

ACKNOWLEDGMENTS

The authors thank the CAMD staff for their assistance, and (E.D.P.) acknowledges support from NSF (Grant No. CHE-9616908). The work at Caltech was also supported in part by the National Science Foundation.

[1] K. Wang and V. McKoy, Annu. Rev. Phys. Chem. **46**, 275 (1995).
[2] R. R. Lucchese, K. Takatsuka, and V. McKoy, Phys. Rep. **131**, 147 (1986).
[3] V. McKoy, T. A. Carlson, and R. R. Lucchese, J. Phys. Chem. **88**, 3188 (1984).
[4] J. W. Copper, Phys. Rev. **128**, 681 (1962).
[5] S. T. Manson, Phys. Rev. A **31**, 3698 (1985).
[6] T. A. Carlson, A. Fahlman, M. O. Krause, T. A. Whitley, and F. A. Grimm, J. Chem. Phys. **81**, 5389 (1984).
[7] T. A. Carlson, A. Fahlman, M. O. Krause, P. R. Keller, J. W. Taylor, T. Whitley, and F. A. Grimm, J. Chem. Phys. **80**, 3521 (1984).
[8] T. A. Carlson, M. O. Krause, W. A. Svensson, P. Gerard, F. A. Grimm, T. A. Whitley, and B. P. Pullen, Z. Phys. D: At., Mol. Clusters **2**, 309 (1986).
[9] J. L. Dehmer, J. Chem. Phys. **56**, 4496 (1972).
[10] J. L. Dehmer and D. Dill, Phys. Rev. Lett. **35**, 213 (1975).
[11] J. L. Dehmer and D. Dill, J. Chem. Phys. **65**, 5327 (1977).
[12] D. Loomba, S. Wallace, D. Dill, and J. L. Dehmer, J. Chem. Phys. **75**, 4546 (1981).
[13] M. N. Piancastelli, J. Electron Spectrosc. Relat. Phenom. **100**, 167 (1999).
[14] M. N. Piancastelli, P. R. Keller, J. W. Taylor, F. A. Grimm, T. A. Carlson, M. O. Krause, and D. Lichtenberger, J. Electron Spectrosc. Relat. Phenom. **34**, 205 (1984).
[15] S. Kakar, E. D. Poliakoff, and R. A. Rosenberg, J. Chem. Phys. **96**, 23 (1992).
[16] L. A. Kelly, L. M. Duffy, B. Space, E. D. Poliakoff, P. Roy, S. H. Southworth, and M. G. White, J. Chem. Phys. **90**, 1554 (1989).
[17] R. G. Tonkyn, J. W. Winniczek, and M. G. White, Chem. Phys. Lett. **164**, 137 (1989).
[18] R. T. Wiedmann, E. R. Grant, R. G. Tonkyn, and M. G. White, J. Chem. Phys. **95**, 746 (1991).
[19] E. R. Grant and M. G. White, Nature (London) **354**, 249 (1991).
[20] R. T. Wiedmann, M. G. White, K. Wang, and V. McKoy, J. Chem. Phys. **100**, 4738 (1994).
[21] R. T. Wiedmann and M. G. White, J. Chem. Phys. **102**, 5141 (1995).
[22] R. T. Wiedmann, M. G. White, H. Lefebvre-Brion, and C. Cossart-Magos, J. Chem. Phys. **103**, 10417 (1995).
[23] W. Kong and J. W. Hepburn, Int. J. Mass Spectrom. Ion Processes **159**, 27 (1996).
[24] R. Signorell and F. Merkt, J. Chem. Phys. **110**, 2309 (1999).
[25] J. Xie and R. N. Zare, Chem. Phys. Lett. **159**, 399 (1989).
[26] H. Park and R. N. Zare, J. Chem. Phys. **104**, 4554 (1996).
[27] H. Park, D. J. Leahy, and R. N. Zare, Phys. Rev. Lett. **76**, 1591 (1996).
[28] G. Ohrwall, P. Baltzer, and J. Bozek, Phys. Rev. A **59**, 1903 (1999).
[29] G. Ohrwall, P. Baltzer, and J. Bozek, Phys. Rev. Lett. **81**, 546 (1998).
[30] E. D. Poliakoff, J. C. K. Chan, and M. G. White, J. Chem. Phys. **85**, 6232 (1986).
[31] S. Kakar, H.-C. Choi, and E. D. Poliakoff, J. Chem. Phys. **97**, 6998 (1992).
[32] H. C. Choi, R. M. Rao, A. G. Mihill, S. Kakar, E. D. Poliakoff, K. Wang, and V. McKoy, Phys. Rev. Lett. **72**, 44 (1994).
[33] E. D. Poliakoff, H. C. Choi, R. M. Rao, A. G. Mihill, S. Kakar, K. Wang, and V. Mckoy, J. Chem. Phys. **103**, 1773 (1995).
[34] E. D. Poliakoff and R. M. Rao, J. Electron Spectrosc. Relat. Phenom. **79**, 361 (1996).
[35] R. M. Rao, E. D. Poliakoff, K. Wang, and V. McKoy, J. Chem. Phys. **104**, 9654 (1996).
[36] E. D. Poliakoff, M.-H. Ho, G. E. Leroi, and M. G. White, J. Chem. Phys. **84**, 4779 (1986).
[37] R. Rao, Ph. D. dissertation, Louisiana State University and Agricultural and Mechanical College, 1996.
[38] M. Braunstein, V. McKoy, S. N. Dixit, R. G. Tonkyn, and M. G. White, J. Chem. Phys. **93**, 5345 (1990).
[39] J. W. Hepburn, J. Chem. Phys. **107**, 7106 (1997).
[40] K. Müller-Dethlefs and E. W. Schlag, Annu. Rev. Phys. Chem. **42**, 109 (1991).
[41] R. Signorell and F. Merkt, Faraday Discuss. **115**, 351 (2000).
[42] M. Evans and C. Y. Ng, J. Chem. Phys. **111**, 8879 (1999).
[43] J. C. Huang, Y. S. Cheung, M. Evans, C. X. Liao, C. Y. Ng, C. W. Hsu, P. Heimann, H. LefebvreBrion, and C. CossartMagos, J. Chem. Phys. **106**, 864 (1997).
[44] G. K. Jarvis, M. Evans, C. Y. Ng, and K. Mitsuke, J. Chem. Phys. **111**, 3058 (1999).
[45] G. K. Jarvis, Y. Song, and C. Y. Ng, J. Chem. Phys. **111**, 1937 (1999).
[46] G. K. Jarvis, Y. Song, and C. Y. Ng, Rev. Sci. Instrum. **70**, 2615 (1999).
[47] J. B. Liu, W. W. Chen, C. W. Hsu, M. Hochlaf, M. Evans, S. Stimson, and C. Y. Ng, J. Chem. Phys. **112**, 10767 (2000).
[48] J. B. Liu, M. Hochlaf, and C. Y. Ng, J. Chem. Phys. **113**, 7988 (2000).
[49] Y. Song, M. Evans, C. Y. Ng, C. W. Hsu, and G. K. Jarvis, J. Chem. Phys. **111**, 1905 (1999).
[50] S. Stimson, M. Evans, C. Y. Ng, C. W. Hsu, P. Heimann, C. Destandau, G. Chambaud, and P. Rosmus, J. Chem. Phys. **108**, 6205 (1998).
[51] K. Suzuki, Y. Emura, S. Ishiuchi, and M. Fujii, J. Electron Spectrosc. Relat. Phenom. **108**, 13 (2000).
[52] K. H. Wang, D. A. Rodham, V. McKoy, and G. A. Blake, J. Chem. Phys. **108**, 4817 (1998).
[53] W. G. Wilson, K. S. Viswanathan, E. Sekreta, and J. P. Reilly, J. Phys. Chem. **88**, 672 (1984).
[54] X. Song, E. Sekreta, J. P. Reilly, H. Rudolph, and V. McKoy, J. Chem. Phys. **91**, 6062 (1989).
[55] H. Park and R. N. Zare, J. Chem. Phys. **104**, 4568 (1996).
[56] A. M. Rijs, E. H. G. Backus, C. A. de Lange, M. H. M. Janssen, K. Wang, and V. McKoy, J. Chem. Phys. **114**, 9413 (2001).
[57] J. B. Milan, W. J. Buma, C. A. d. Lange, K. Wang, and V. McKoy, J. Chem. Phys. **103**, 3262 (1995).
[58] J. G. Underwood and K. L. Reid, J. Chem. Phys. **113**, 1067 (2000).
[59] D. Townsend and K. L. Reid, J. Chem. Phys. **112**, 9783 (2000).
[60] K. L. Reid and J. G. Underwood, J. Chem. Phys. **112**, 3643 (2000).
[61] K. L. Reid, T. A. Field, M. Towrie, and P. Matousek, J. Chem. Phys. **111**, 1438 (1999).
[62] J. S. Miller, E. D. Poliakoff, T. F. Miller, A. P. P. Natalense, and R. R. Lucchese, J. Chem. Phys. **114**, 4496 (2001).
[63] B. C. Craft, M. Feldman, E. Morikawa, E. D. Poliakoff, V. Saile, J. D. Scott, and R. L. Stockbauer, Rev. Sci. Instrum. **63**, 1561 (1992).
[64] E. Morikawa, J. D. Scott, E. D. Poliakoff, R. L. Stockbauer, and V. Saile, Rev. Sci. Instrum. **63**, 1300 (1992).
[65] K. Wang and V. McKoy, J. Chem. Phys. **95**, 4977 (1991).
[66] W. Kong, D. Rodgers, J. W. Hepburn, K. Wang, and V. McKoy, J. Chem. Phys. **99**, 3159 (1993).
[67] R. Das, C. Y. Wu, A. G. Mihill, E. D. Poliakoff, K. S. Wang, and V. McKoy, J. Chem. Phys. **101**, 5402 (1994).
[68] R. Das, C. Wu, A. G. Mihill, E. D. Poliakoff, K. Wang, and V. McKoy, J. Phys. Chem. **99**, 1741 (1994).
[69] J. L. Dehmer, D. Dill, and S. Wallace, Phys. Rev. Lett. **43**, 1005 (1979).
[70] J. B. West, A. C. Parr, B. E. Cole, D. L. Ederer, R. Stockbauer, and J. L. Dehmer, J. Phys. B **13**, L105 (1980).